Astrovirus Disrupts Intestinal Barrier Function by Activating Epithelial-Mesenchymal Transition

Astrovirus Infection Induces EMT

Virginia Hargest,[1] Geoffrey Neale,[2] and Stacey Schultz-Cherry[1,*]

[1] Department of Infectious Diseases, St. Jude Children's Research Hospital, Memphis, TN 38105, USA

[2] Hartwell Center for Bioinformatics and Biotechnology, St. Jude Children's Research Hospital, Memphis, TN 38105, USA

* Corresponding author: stacey.schultz-cherry@stjude.org

Author contributions: Conceptualization, V.H. and S.S.C.; data curation, V.H. and G.N.; formal analysis, V.H. and G.N.; funding acquisition, S.S.C.; investigation, V.H.; methodology, V.H.; project administration, S.S.C.; supervision, S.S.C.; visualization, V.H.; writing—original draft preparation, V.H. and S.S.C; writing—review and editing, all authors.

Abstract

Human astroviruses (HAstV), positive sense single-stranded RNA viruses, are one of the leading causes of diarrhea worldwide. Despite their high prevalence, the cellular mechanisms of astrovirus pathogenesis remain ill-defined. Previous studies showed HAstV increased epithelial barrier permeability by causing a relocalization of the tight junction protein, occludin. In these studies, we demonstrate that HAstV infection induces epithelial-mesenchymal transition (EMT), by upregulation the transcription of EMT-related genes within 8 hours post-infection (hpi), followed by the loss of cell-cell contacts and disruption of polarity by 24 hpi. Unlike the relocalization of tight junction proteins, HAstV-induced EMT requires productive replication and is independent of cellular factors including transforming growth factor-β (TGF-β). While multiple classical HAstV serotypes, including clinical isolates, induce EMT, the non-classical genotype HAstV-VA1 and two strains of reovirus are incapable of inducing EMT. This finding puts classical strains of HAstV-1 in an exclusive group of non-oncogenic viruses triggering EMT.

Author Summary

While human astroviruses (HAstV) were discovered nearly 45 years ago, these small positive-sense RNA viruses remain critically understudied, leaving us with limited knowledge of its pathogenesis. This study fills the gap in knowledge demonstrating that HAstV are among a select group of viruses that induce epithelial-mesenchymal transition (EMT). Here we demonstrate that HAstV-1 replication induces transcriptional and phenotypic changes in intestinal epithelial cells associated with EMT. Additionally, we show inducing EMT is not common to enteric RNA viruses, as reovirus strains were found to be incapable of inducing EMT. Unlike the viruses that are known to induce EMT, astrovirus infection is not associated with cancer. We hypothesize that our findings will extend beyond astrovirus and may shed light on novel ways viruses can circumvent the barriers meant to protect against them.

Introduction

Epithelial and mesenchymal cells share inherent plasticity that allows for switching between the two cell states through a biological process known as epithelial-mesenchymal transition (EMT). EMT is essential in the development, differentiation, and repair of tissues and organs; however, EMT can negatively contribute to organ fibrosis and the initiation of cancerous metastases. EMT has been shown to induce stem cell properties [1,2], prevent apoptosis and senescence [3–5], and contribute to immunosuppression [6]. The complex process of EMT involves extensive reprogramming of gene expression, which can be regulated by numerous signaling pathways [7]. Activation of these signaling pathways ultimately results in the upregulation of the transcription factors including Snail1/2, Twist, and ZEB1/2 [7]. These transcription factors negatively regulate epithelial markers such as occludin, claudins, and E-cadherin, while positively regulating mesenchymal genes like N-cadherin, fibronectin, and vimentin [8]. This allows for the hallmark phenotypic changes associated with EMT like the disassembly of the epithelial cell-cell junctions, the loss of apical-basal polarity, and the formation of lamellipodia or filopodia to enable migration [9].

Epithelial cells that line the intestinal lumen function as a barrier that absorbs nutrients and electrolytes while restricting entry of harmful substances or pathogens [10]. Breaches in this barrier by death of the epithelial cells or disruption of cellular junctions through non-cytopathic mechanisms are associated with gastrointestinal diseases including irritable bowel syndrome, Crohn's disease, and colitis [11]. Along with these diseases, enteric viruses are known to compromise the gastrointestinal barrier. Human astroviruses (HAstV), small, non-enveloped positive-sense single-stranded RNA viruses, have been shown to predominantly infect differentiated epithelial cells at the tips of the intestinal villi [12,13]. We have demonstrated that astrovirus disrupts the intestinal barrier through a novel mechanism independent of cellular damage or induction of the host inflammatory response [14–16]. Instead, astroviruses increase barrier permeability by inducing the relocalization of the tight junction protein occludin [15]. The

relocalization of occludin by astrovirus does not require productive infection; the viral capsid protein alone is sufficient to cause disruption *in vivo* and *in vitro* [15,16]. Because loss of cell junctions is a phenotypic hallmark of EMT, we hypothesized that HAstV may serve as a viral trigger of EMT.

Indeed, several viruses are known to induce EMT including hepatitis B virus (HBV) [17], hepatitis C virus (HCV) [18], human papilloma virus (HPV) [19], Epstein-Barr virus (EBV) [20], and cytomegalovirus (CMV) [21,22]. These viruses, unlike HAstV, are oncogenic, and EMT induction leads to metastases, hepatocellular carcinoma, cervical carcinomas, and lymphoma among other diseases. Here, we demonstrate that HAstV is a non-oncogenic virus that also drives EMT. HAstV-induced EMT begins with an upregulation of EMT related genes and transcription factors at 8 hours post-infection (hpi). This is followed by a loss of epithelial cell-specific genes and proteins and gain of mesenchymal proteins like vimentin by 24 hpi. It is also accompanied by a loss of cellular polarity. Intriguingly, we demonstrate that HAstV activates TGF-β, a well-established inducer of EMT. However, HAstV-induced EMT is independent of TGF-β signaling but is dependent on productive viral replication. While multiple classical HAstV serotypes are capable of inducing EMT, other enteric viruses and even non-classical HAstV genotypes do not trigger EMT. The studies described here are amongst the first to demonstrate that a non-oncogenic virus drives EMT.

Results

HAstV infection leads to EMT-associated gene modulation

We have previously demonstrated that HAstV-1 leads to reorganization of occludin and the actin cytoskeleton without causing cell death [15]. This observation led us to hypothesize that HAstV infection induces EMT. Since EMT is a transcriptionally regulated process, we sought to determine if EMT-associated genes were modulated during HAstV-1 infection by first

performing microarray analysis. Gene set enrichment analysis (GSEA) of the microarray data demonstrated that several pathways were significantly upregulated in HAstV-infected versus uninfected Caco-2 cells at 24 hpi, including the EMT pathway (Figure S1). To investigate this further, we performed more targeted quantitative analysis by examining mRNA levels of EMT associated genes throughout infection by multiplexed qRT-PCR using Qiagen's RT^2 Profiler system (Figure S2). Cellular pathways associated with the induction of EMT were upregulated at 8 hpi including, Wnt, TGF-β, and Notch, as were specific transcription factors known to drive EMT including Snail, ZEB1/2, and Twist. We validated the RT^2 Profiler findings by quantitating mRNA levels of EMT-related transcription factors as well as E-cadherin (*CDH1*), occludin (*OCLN*), Snail (*SNAI1*), and vimentin (*VIM*) by qRT-PCR. We observed an upregulation of the EMT-related transcription factors *SNAI1*, *TWIST1*, *ZEB1*, and *ZEB2* around 4hpi (Figure 1A). The activation of these transcription factors was followed by the downregulation of epithelial genes, *CDH1* and *OCLN*, as early as 8 hpi and the upregulation of mesenchymal gene *VIM* by 24 hpi (Figure 1B). The upregulation of *SNAI1* was not sustained throughout infection but instead may be regulated in a biphasic manner as another increase in mRNA level was observed at 24hpi (Figure 1B).

HAstV infection leads to a time-dependent reorganization and decrease in junctional protein levels.

Given the transcriptional changes, we asked if junctional protein expression was also disrupted during HAstV infection. To examine this, Caco-2 grown on glass coverslips were infected with HAstV-1 and stained for tight junction proteins, occludin and zonula occludens-1 (ZO-1), and adherens junction proteins, E-cadherin and β-catenin, at 6, 12, 18, and 24 hpi. Mock-infected cells showed normal cell junction morphology, with a cobblestone-like staining pattern as protein localization was restricted to the cell periphery. However, HAstV-infected cells had disrupted junctional proteins. The disruption was as early as 6hpi with occludin beginning to re-localize away from the cell periphery (Figure 2A). Re-localization of occludin was followed by

ZO-1 moving from the cell membrane around 18 hpi. The most striking finding was the reorganization of E-cadherin, a key marker of epithelial cells [23], by 18 hpi. E-cadherin is crucial in the establishment and maintenance of the cellular junction complex as a whole [24,25], and aberrant expression of E-cadherin is a hallmark of epithelial dysregulation [7]. Additionally, we observed an increase in vimentin staining correlating to the increase in vimentin mRNA. Not only did we observe cellular junction reorganization, but the overall proteins levels were also decreased. Over the course of 24 hours, expression of the junctional proteins occludin ($p<0.0001$), E-cadherin ($p<0.0001$), ZO-1 ($p=0.0058$), and β-catenin ($p=0.0139$) were all significantly decreased relative to mock-infected cells (Figure 2B, C), indicating the observed transcriptional changes during HAstV infection translated to a decrease in junctional protein expression.

HAstV-induced EMT disrupts cellular polarity

Cellular junctions act as a physical barrier that prevent the movement of lipids and membrane proteins from migrating between the apical and basolateral cell membranes [26].When cellular junctions are disassembled, proteins that were once localized to the basolateral membrane freely migrate to the apical side causing a loss of cellular polarity [27]. To determine if cellular polarity was disrupted during HAstV-1 infection, we stained for ezrin, a cytoplasmic linker between the apical membrane and the actin cytoskeleton [28], and sodium-potassium ATPase (Na/K-ATPase), a transporter localized to the basolateral membrane [29]. In mock-infected cells ezrin was distinctly localized to the apical side and Na/K-ATPase to the basolateral with very little overlap (Figure 3A). However, by 24 hpi there was less organized arrangement for both proteins. To quantitate the disruption of polarity, we measured the amount of Na/K-ATPase at apical membrane. At 24 hpi, there was significantly more Na/K-ATPase located at the apical membrane than in mock-infected cells (Figure 3B, C). We also noticed that cells appeared to lift or be extruded from the cell monolayer (Figure 3A; bottom panel). The transcriptional reprogramming, disassembly of epithelial cell-cell contacts, especially the

disruption and decreased production of E-cadherin, and disruption of cellular polarity all indicated that during HAstV-1 infection cells were undergoing EMT.

TGF-β activity is increased during HAstV infection but isn't involved in HAstV-induced EMT

We next asked what viral and/or cellular factors were involved in HAstV-induced EMT. When examining the upregulation of mesenchymal genes, we observed that TGF-β mRNA was increased at both 8 and 24 hpi (Figure S2). Since TGF-β is the classical activator of EMT [7,30,31], we asked whether this increase in mRNA translated to an increase in TGF-β activity. To measure active TGF-β levels, we utilized a specific biological reporter assay where mink lung epithelial cells (Mv1Lu) stably express the PAI promoter upstream of luciferase [32]. Supernatants collected from HAstV-1 infected Caco-2 cells between 4 and 24 hpi were added to the Mv1Lu-PAI cells and TGF-β activity was quantitated. Supernatants from HAstV-1- infected cells contained significantly more active TGF-β compared to mock-infected cells beginning at 6 hpi and peaking at 12 hpi (Figure 4A). We also observed an increase in SMAD3 nuclear localization in HAstV-1-infected cells comparable to cells treated with TGF-β alone and upregulation of *SERPINE1* mRNA, which is specifically activated by TGF-β, mRNA at 24hpi (Figure 4B, C). These studies demonstrate that astrovirus infection leads to an increase in biologically active TGF-β.

To determine if HAstV-induced EMT was dependent on this active TGF-β, TGF-β signaling was inhibited using the small molecule inhibitor SB431542 [33], which selectively inhibits the phosphorylation of the TGF-β type I receptor. Despite inhibiting TGF-β signaling, SB431542 had no impact on HAstV-1-induced transcriptional regulation of genes associated with EMT (Figure 5A), and failed to restore E-cadherin protein expression (Figure 5B). This was not an unexpected result. Previous research showed that TGF-β1 does not easily induce EMT in Caco-2 cells [34]. Indeed, we found that the addition of 20 ng/ml TGF-β1 did not induce EMT

within the same time frame as HAstV. The loss of E-cadherin and disruption of polarity was not seen until 3 days following TGF-β administration (Figure S3) suggesting that activation of TGF-β during infection is not the primary mechanism for HAstV-induced EMT. However, we cannot discount the possibility that TGF-β plays a critical role in EMT induction *in vivo,* as we have shown TAstV-2 infection in turkey poults also causes an increase in TGF-β activity [14].

HAstV-induced EMT is dependent on viral replication

Since the canonical cellular pathway for EMT induction was not involved in HAstV-induced EMT, we sought to determine if a viral factor was involved. When we performed the microarray analysis on infected and non-infected cells (Figure S1), we also performed an analysis on various differentiation states of uninfected Caco-2 cells given that less differentiated cells are less permissive to HAstV infection. Intriguingly, we found the EMT pathway was significantly downregulated in differentiated cells which are highly permissive to HAstV infection (Figure S4). This indicated that the EMT pathway is not associated with cellular differentiation and supported our hypothesis that it is induced by viral infection. To test this, we inoculated Caco-2 cells with UV-inactivated virus and assessed the hallmarks of EMT. UV-inactivated virus did not increase *SNAI1* mRNA, decrease *CDH1* leading to reduced E-cadherin expression, or disrupt cellular polarity (Figure 6A-C). Further, inhibition of ERK1/2, which is critical for HAstV replication [35], with U0126, rescued more than 27% of E-cadherin expression and cellular polarity (Figure 6D,E). These studies suggest that productive replication is required for the induction of EMT.

The induction of EMT is unique to HAstV

All of the previous studies were performed using a lab-adapted strain of HAstV-1, we next determined the breadth of HAstV strains capable of inducing EMT. Caco-2 cells were infected with three classical HAstVs isolated from patient samples, SJ054.225 (HAstV-1), SJ60.212 (HAstV-8), and SJ177.110 (HAstV-2), as well as lab adapted classical serotypes HAstV-8 and HAstV-2. All clinical isolates and lab-adapted serotypes disrupted the localization

(Figure 7A) and expression (Figure 7B) of E-cadherin. Additionally, infection with these viruses disrupted polarity as demonstrated by re-localization of both ezrin and Na/K ATPase (Figure 7C). In contrast, the non-classical HAstV-VA1 genotype, which shares only 33% homology with HAstV-1 [36], failed to downregulate *CDH1* or upregulate *SNAI1* or *TWIST1* (Figure 8A) despite productively replicating in the Caco-2 cells (Figure 8B). The lack of EMT was not unique to HAstV-VA1. Reovirus stains T1L and T3SA+, while also productively replicated in Caco-2 cells, failed to disrupt E-cadherin protein localization (Figure 8B) or expression (Figure 8C). Finally, neither reovirus strain nor HAstV-VA1 were able to disrupt cellular polarity upon infection (Figure 8D). This shows classical HAstV is distinct among other enteric RNA viruses in the ability to induce EMT.

Discussion

In these studies, we demonstrate that HAstV replication triggers EMT in Caco-2 cells. Mechanistically, HAstV-induced EMT is driven by transcriptional changes; specifically, the downregulation of *CDH1* and *OCLN* and the upregulation of the key transcriptional factor *SNAI1* early after infection. These transcriptional changes result in decreased epithelial protein levels, leading to a breakdown of the cell junctions, the loss of cellular polarity, and upregulation of mesenchymal cell-specific genes like *VIM* by 24 hpi. Despite an increase in active TGF-β during HAstV infection, inhibition of TGF-β signaling did not prevent the EMT phenotype. Instead the data we present showed that HAstV replication causes the transcriptional reprogramming associated with EMT.

While multiple classical HAstV serotypes induced EMT, this was not true of all astrovirus genotypes. HAstV-VA1 failed to drive EMT despite productively replicating in Caco-2 cells. We showed that HAstV-VA1 failed to upregulate the transcription factor *SNAI1* during a 24-hour infection. The lack of *SNAI1* regulation is a key finding as we observed multiple waves of *SNAI1*

upregulation with HAstV-1 infection (Figure 1), which is likely a driving force in HAstV-induced EMT. HAstV-VA1 is a non-classical HAstV strain, genetically more related to mink and ovine astroviruses than to the classical human serotypes [37–39]. Unlike classical HAstVs, HAstV-VA1 has rarely been linked to diarrhea [40,41] but has been reported in association with neurological disease [36,42]. Classical and non-classical HAstVs are genetically distinct and differ on key factors of replication and pathogenesis [43,44]. Since the novel HAstV strain was discovered just over 10 years ago, investigations into its pathogenesis are just beginning and our finding that it does not induce EMT may reveal an underlying fundamental difference between it and classical HAstVs.

The induction of EMT is also not a characteristic of other enteric RNA viruses. Reovirus, like HAstV, is a small RNA virus that can cause severe diarrhea in children [45]. Yet, two separate strains of reovirus were unable to cause the same phenotypic or transcriptional hallmarks of EMT. Attempts to examine coxsackievirus (CVB3)-induced EMT were unsuccessful due to the cytopathogenic nature of this virus. The lack of EMT induction by other enteric viruses also indicates this is not a phenomenon the Caco-2 cell line used as our *in vitro* model. Since Caco-2 cells are a carcinoma cell line, it could be suggested these cells are simply predisposed to undergo EMT. However, all viral infections were carried out under the same conditions in the Caco-2 cell line. Given the other viral stains did not induce EMT, our findings are not an artifact of the cells. EMT is a rare phenomenon triggered by only a few viruses and even less non-oncogenic viruses, making HAstV-induced EMT a truly unique finding.

Although our data suggests that TGF-β is likely not the main mechanism utilized by HAstV to induce EMT, we believe it is still an important factor in astrovirus pathogenesis. TGF-β is upregulated in activity both *in vitro* and *in vivo* [14], so it must be an integral part of the viral pathogenesis. Interestingly, our SMAD3 staining showed that TGF-β signaling is mostly occurring in non-infected cells in the epithelial monolayer. This bystander effect is likely very

important *in vivo* where TGF-β can create an immune suppressive microenvironment [46] and could account for the lack of inflammation see in *in vivo* astrovirus infections. Future studies will look at the role of TGF-β activation in astrovirus replication.

Here we show that HAstV replication is triggering the transcriptional changes necessary for the induction of EMT. Using GSEA, we found Caco-2 cells that are highly permissive to HAstV infection significantly downregulated the EMT pathway (Figure S4). This is understandable as untreated cells do not undergo EMT and Caco-2 cells do not lose contact inhibition even after weeks in culture [47]. However, following HAstV-1 infection the EMT pathway was significantly upregulated, it indicated to us this pathway was induced by HAstV infection itself (Figure S1). Our previous research has shown the astrovirus capsid alone can increase barrier permeability and disrupt cellular junctions *in vitro* and *in vivo* [15,16]. Conversely, when HAstV-1 is UV-inactivated, preventing the virus from replicating its genome, it no longer is capable of inducing EMT. Additionally, when viral replication was suppressed using the ERK1/2 inhibitor U0126, we saw a decline in the hallmarks of EMT. The addition of U0126 to HAstV infection did not completely reverse the effects of EMT, however this was expected as U0126 does not completely inhibit HAstV replication [35]. We hypothesize that there may be a binding event that is sufficient to cause some barrier permeability and the re-localization of occludin thus allowing the capsid protein alone to cause these events. However, a more intricate signaling cascade is triggered during replication of the virus that induces the EMT phenotype. While further research is needed to determine the exact aspect of replication that is initiating EMT, our current hypothesis is the production and activity of one of the HAstV non-structural proteins is involved.

Although the cleavage process of the HAstV nonstructural polyproteins is still not well characterized, it has been suggested at least four nonstructural proteins in addition to an RNA-dependent RNA polymerase (RdRp) are produced during replication [12]. However, the exact

function of these nonstructural proteins remains undetermined. It has been shown that genetic variation in at least one of the HAstV nonstructural proteins can impact viral RNA production and the amount of infectious virus shed [48,49]. Studies of the oncogenic viruses that induce EMT have shown strong evidence that viral proteins are heavily involved. The X protein of HBV [17,50–52], NS4B [53] and core protein of HCV [54–56], E5 [57] and E6/E7 oncoproteins of HPV [58,59], nuclear antigens [60] and latent membrane proteins of EBV [61–63], and immediate early proteins 1 and 2 of CMV [21] have all been shown to act as transcription factors inducing EMT. Given this, it is possible one of the nonstructural proteins or a cleavage product may impact the induction of EMT during HAstV infection. While we currently lack the tools necessary for additional studies focused on the nonstructural proteins, these studies will be critical in order to definitively identify if viral proteins are involved in HAstV-induced EMT.

In conclusion, we demonstrated HAstV replication induces EMT. To date, HAstV infection has not been associated as a risk factor for developing any type of cancer. This makes astrovirus unique as the majority of viruses known to induce EMT are oncogenic [64]. The data presented here not only provides increased knowledge on astrovirus pathogenesis but also induction of EMT from by a non-oncogenic virus. Studies are underway to examine what effect EMT has on astrovirus replication and if this process contributes to disease *in vivo.*

Materials and Methods

Cells and Virus Propagation

The human intestinal adenocarcinoma cell line Caco-2 was obtained from ATCC (HTB-37). Cells were propagated in minimum essential medium (MEM; Corning) supplemented with 20% fetal bovine serum (FBS; HyClone), GlutaMax-I (Gibco), and 1 mM sodium pyruvate (Gibco). HAstV-1, HAstV-2, and HAstV-8 lab adapted viral stocks were propagated in Caco-2 cells. Infectious titers were quantitated on Caco-2 cells by the fluorescent-focus assay as previously described [65].

To UV inactivate the virus, 100 µl of HAstV-1 was subjected to 100 mJ/cm^2 with a UV cross-linker as described previously [15]. Inactivation was confirmed by the fluorescent-focus assay. Clinical isolates (SJ054.225, SJ60.212, and SJ177.110) were isolated as previously described [66].

The reovirus T1l and T3SA+ strains were generous gifts from Dr. Terence Dermody's lab at the University of Pittsburgh. HAstV-VA1 was a gift from Dr. David Wang's lab at Washington University in St. Louis.

Immunofluorescent Staining

Briefly, Caco-2 cells were seeded onto glass coverslips (for epithelial and vimentin staining) or transwells (polarity and SMAD3 staining). Once confluent, the cells were infected with HAstV-1 (MOI 10) or mock infected. At various times post-infection, cells were fixed with 4% paraformaldehyde (for epithelial and vimentin staining) or 100% ice cold methanol (polarity and SMAD3 staining), and then blocked with 5% normal goat serum (NGS) in PBS at room temperature for 1 hour. The cells were stained for E-cadherin (33-4000; Invitrogen), occludin (71-1500; Invitrogen), ZO-1 (33-9100 and 61-7300; Invitrogen), sodium-potassium ATPase (ab167390; abcam), ezrin (MA5-13862; Invitrogen), β-catenin (ab32572; abcam), SMAD3 (51-1500; Invitrogen), HAstV capsid (8e7; DakoCytomation), and vimentin (ab92547; abcam) for 1 hour followed by anti-mouse IgG-Alexa Fluor 488 or anti-rabbit IgG-Alexa Fluor 555 (Invitrogen) secondary antibodies and DAPI (4′,6′-diamidino-2-phenylindole; Sigma) in 1% NGS for 30 min at room temperature. Following staining, coverslips or transwells were mounted onto slides with Prolong Gold Antifade Mountant (Invitrogen) and sealed. Cells were imaged with a Nikon TE2000 inverted microscope Images were captured with a Nikon 60x objective lens using Nikon NIS Elements software.

Western Blotting

Caco-2 cells were mock- or HAstV-1 (MOI 10) infected or were treated with an equal amount of UV-inactivated virus. At the indicated times, monolayers were lysed in 100 µl of RIPA buffer

(Abcam) and 1× protease inhibitor cocktail (Pierce) for 15 min at room temperature and centrifuged at 14,000 × *g* for 5 min at 4°C. Protein concentrations were determined using the BCA Protein Assay Kit (Pierce). Equal protein concentrations of the soluble fraction were separated by sodium dodecyl sulfate-polyacrylamide gel electrophoresis (SDS-PAGE) (4-20%) under reducing conditions. Following transfer to nitrocellulose and probing for for E-cadherin (33-4000; Invitrogen), occludin (71-1500; Invitrogen), ZO-1 (33-9100; Invitrogen), β-catenin (ab32572; abcam), vimentin (ab92547; abcam), and β-actin (A5441; Sigma). The blot was imaged on Licor Odyssey Fc and band densitometry was measured using Image Studio version 5.2 software.

Gene Expression Analysis by Microarray

Total RNA (100 ng) was converted to biotin-labeled cDNA using the Affymetrix WT Plus kit and hybridized to an Affymetrix Human Gene 2.0 ST GeneChip array (Life Technologies). Array probes were normalized and summarized to transcript-level signals by the RMA algorithm using the Affymetrix Expression Console software v1.1. Gene Set Enrichment Analysis (GSEA) was performed as described [67] using gene sets downloaded from MSigDB (https://www.gsea-msigdb.org/gsea/msigdb).

RT² Profiler

Briefly, cells were seeded in 6-well plate, mock infected or HAstV-1 (MOI of 10) infected and collected at the indicated time point in TRIzol reagent (Thermo Fisher Scientific). Then, RNA was isolated according to the manufacturer's instructions. RNA quality was determined and was reverse transcribed using Qiagen's RT² First Strand Kit (Cat# 330401). The cDNA was used on the real-time RT² Profiler PCR Array (Cat# PAHS-090Z) in combination with RT² SYBR Green qPCR Mastermix (Cat# 330529). The CT values were then uploaded on to the data analysis web portal at http://www.qiagen.com/geneglobe. Samples were assigned to either control or test groups. The data was normalized based on a manual selection from full panel of reference

362 genes. The data analysis web portal calculated fold change/regulation using ΔΔCT method, in
363 which ΔCT is calculated between gene of interest and an average of reference genes (B2M,
364 HPRT1, and RPLP0), followed by ΔΔCT calculations (ΔCT (Test Group)-ΔCT (Control Group)).
365 Fold Change was then calculated using 2^(-ΔΔCT) formula.

366 RT-PCR

367 Caco-2 cells were infected with HAstV-1 or mock infected and RNA extracted at indicated
368 timepoints using TRIzol (AMbion) according to manufacturer's specifications. Then qRT-PCR
369 was performed using the QuantiTect SYBR green kit (Qiagen) primer assays for *OCLN* (cat#
370 QT00081844), *CDH1* (cat# QT00080143), *SNAI1* (cat# QT00010010), *TWIST1* (cat#
371 QT00011956), *ZEB1* (cat# QT00020972), *ZEB2* (cat# QT00008554), and *VIM1* (cat#
372 QT00095795). The resulting Ct values were normalized to *GAPDH* (cat# QT00079247). The log
373 transformed ΔΔCt values are reported as fold changes over untreated.

374 Quantification of Sodium Potassium ATPase Staining

375 Following immunofluorescent staining and imaging, basal or apical localization of sodium-
376 potassium ATPase was determined by measuring mean fluorescent intensity above and below
377 cell midline using ImageJ 1.50i software. Results were expressed as a ratio of basal fluorescent
378 intensity to apical fluorescent intensity.

379 TGF-β Activity Assay

380 TGF-β activity was measured using a luciferase reporter cell line, as previously described [32].
381 Briefly, mink lung epithelial cells (Mv1Lu), stably transfected with a luciferase reporter construct
382 downstream of the plasminogen activator inhibitor-1 (PAI-1) promotor, were plated in a 96-well
383 tissue culture plate ($2x10^4$). These cells were inoculated with supernatants (100 μl) taken from
384 HAstV-1 (MOI 10) or mock-infected Caco-2 cells at various times post-infection and incubated
385 at 37°C for 16-20 hours. The inoculum was removed and the cells washed twice with PBS. Cell

lysates were prepared and assayed for luciferase activity using the Luciferase Assay System (Promega) and imaged on the Cytation 5 Cell Imaging Multi-Mode Reader (BioTek).

SB431542 and U0126 Treatment

Briefly, 5×10^4 cells were seeded into transwells (3074; Corning), and once confluent, transferred into serum free media for at least 1 hour. The cells were treated with 10μM SB431542 (Tocris) or U0126 (Promega) 1 hour prior to infection. Then the cells were infected with HAstV-1 (MOI of 5), TGF-β treated (20 ng/ml), or mock infected, according to experiment, in serum free media. Following the virus adsorption period of 1 hour, the inoculum was removed and fresh media containing 10μM SB431542 or U0126 was replaced. DMSO was used as the vehicle control in both experimental setups.

Statistical Analysis

Data were analyzed by ordinary one-way ANOVA (RT-PCR of epithelial and mesenchymal genes), ordinary one-way ANOVA followed by a test for trend (epithelial protein expression), two-tailed student t-test (Na/K-ATPase localization), two-way ANOVA followed by Sidak's multiple comparisons test (TGF-β Activity), ordinary one-way ANOVA followed by Dunnett's multiple comparisons test (E-cad expression with SB431542, UV-inactivated virus, and U0126, and RT-PCR with SB431542 and UV-inactivated virus), using GraphPad Prism version 8. Asterisks show statistical significance as follows: *, $P < 0.05$; **, $P < 0.01$; ***, $P < 0.001$.

Acknowledgments

We would like to thank Jennifer Peters and the St. Jude Light Microscopy Core for their help and guidance with the confocal imaging for this study; Dr. Terence Dermody, Dr. Julie Pfeiffer, and Dr. David Wang for their generous gifts of the reovirus, coxsackievirus, and HAstV-VA1 strains and antibodies, respectively; Rebekah Honce for input on the design of figures. Valerie

Cortez and Victoria Meliopoulos for the isolation and propagation of the HAstV clinical isolates as well as for edits of the manuscript.

This research was supported by NIH grant R21 AI135254-01. The content is solely the responsibility of the authors and does not necessarily represent the official views of the National Institutes of Health. St. Jude Children's Research Hospital Children's Infection Defense Center and ALSAC also provided funding for this work. Images were acquired at the Cell & Tissue Imaging Center which is supported by SJCRH and NCI P30 CA021765. Microarray data were generated in the Hartwell Center for Bioinformatics and Biotechnology which is also supported by P30 CA021765.

Competing interests: Authors declare no competing interests.

Data Availability: All relevant data are within the paper and its Supplementary Materials files. Microarray data has been deposited in the GEO database with accession number GSE166820.

References

1. Mani SA, Guo W, Liao M-J, Eaton EN, Ayyanan A, Zhou AY, et al. The epithelial-mesenchymal transition generates cells with properties of stem cells. Cell. 2008;133: 704–715. doi:10.1016/j.cell.2008.03.027

2. Morel A-P, Lièvre M, Thomas C, Hinkal G, Ansieau S, Puisieux A. Generation of breast cancer stem cells through epithelial-mesenchymal transition. PloS One. 2008;3: e2888. doi:10.1371/journal.pone.0002888

3. Gal A, Sjöblom T, Fedorova L, Imreh S, Beug H, Moustakas A. Sustained TGF beta exposure suppresses Smad and non-Smad signalling in mammary epithelial cells, leading to EMT and inhibition of growth arrest and apoptosis. Oncogene. 2008;27: 1218–1230. doi:10.1038/sj.onc.1210741

4. Thiery JP, Acloque H, Huang RYJ, Nieto MA. Epithelial-Mesenchymal Transitions in Development and Disease. Cell. 2009;139: 871–890. doi:10.1016/j.cell.2009.11.007

5. Ansieau S, Bastid J, Doreau A, Morel A-P, Bouchet BP, Thomas C, et al. Induction of EMT by twist proteins as a collateral effect of tumor-promoting inactivation of premature senescence. Cancer Cell. 2008;14: 79–89. doi:10.1016/j.ccr.2008.06.005

6. Kudo-Saito C, Shirako H, Takeuchi T, Kawakami Y. Cancer metastasis is accelerated through immunosuppression during Snail-induced EMT of cancer cells. Cancer Cell. 2009;15: 195–206. doi:10.1016/j.ccr.2009.01.023

7. Gonzalez DM, Medici D. Signaling mechanisms of the epithelial-mesenchymal transition. Sci Signal. 2014;7: re8. doi:10.1126/scisignal.2005189

8. Lamouille S, Xu J, Derynck R. Molecular mechanisms of epithelial-mesenchymal transition. Nat Rev Mol Cell Biol. 2014;15: 178–196. doi:10.1038/nrm3758

9. Thiery JP, Sleeman JP. Complex networks orchestrate epithelial–mesenchymal transitions. Nat Rev Mol Cell Biol. 2006;7: 131–142. doi:10.1038/nrm1835

10. Ulluwishewa D, Anderson RC, McNabb WC, Moughan PJ, Wells JM, Roy NC. Regulation of tight junction permeability by intestinal bacteria and dietary components. J Nutr. 2011;141: 769–776. doi:10.3945/jn.110.135657

11. Odenwald MA, Turner JR. Intestinal permeability defects: is it time to treat? Clin Gastroenterol Hepatol Off Clin Pract J Am Gastroenterol Assoc. 2013;11: 1075–1083. doi:10.1016/j.cgh.2013.07.001

12. Cortez V, Meliopoulos VA, Karlsson EA, Hargest V, Johnson C, Schultz-Cherry S. Astrovirus Biology and Pathogenesis. Annu Rev Virol. 2017. doi:10.1146/annurev-virology-101416-041742

13. Sebire NJ, Malone M, Shah N, Anderson G, Gaspar HB, Cubitt WD. Pathology of astrovirus associated diarrhoea in a paediatric bone marrow transplant recipient. J Clin Pathol. 2004;57: 1001–1003. doi:10.1136/jcp.2004.017178

14. Koci MD, Moser LA, Kelley LA, Larsen D, Brown CC, Schultz-Cherry S. Astrovirus induces diarrhea in the absence of inflammation and cell death. J Virol. 2003;77: 11798–11808.

15. Moser LA, Carter M, Schultz-Cherry S. Astrovirus increases epithelial barrier permeability independently of viral replication. J Virol. 2007;81: 11937–11945. doi:10.1128/JVI.00942-07

16. Meliopoulos VA, Marvin SA, Freiden P, Moser LA, Nighot P, Ali R, et al. Oral Administration of Astrovirus Capsid Protein Is Sufficient To Induce Acute Diarrhea In Vivo. mBio. 2016;7. doi:10.1128/mBio.01494-16

17. Shin Kim S, Yeom S, Kwak J, Ahn H-J, Lib Jang K. Hepatitis B virus X protein induces epithelial-mesenchymal transition by repressing E-cadherin expression via upregulation of E12/E47. J Gen Virol. 2016;97: 134–143. doi:10.1099/jgv.0.000324

18. Bose SK, Meyer K, Di Bisceglie AM, Ray RB, Ray R. Hepatitis C virus induces epithelial-mesenchymal transition in primary human hepatocytes. J Virol. 2012;86: 13621–13628. doi:10.1128/JVI.02016-12

19. Chamulitrat W, Sattayakhom A, Herold-Mende C, Herold-Mended C, Stremmel W. Human papillomavirus 16 E6/E7-immortalized human gingival keratinocytes with epithelial mesenchymal transition acquire increased expression of cIAP-1, Bclx and p27(Kip1). Exp Dermatol. 2009;18: 1067–1069. doi:10.1111/j.1600-0625.2009.00888.x

20. Horikawa T, Yang J, Kondo S, Yoshizaki T, Joab I, Furukawa M, et al. Twist and epithelial-mesenchymal transition are induced by the EBV oncoprotein latent membrane protein 1 and are associated with metastatic nasopharyngeal carcinoma. Cancer Res. 2007;67: 1970–1978. doi:10.1158/0008-5472.CAN-06-3933

21. Shimamura M, Murphy-Ullrich JE, Britt WJ. Human cytomegalovirus induces TGF-β1 activation in renal tubular epithelial cells after epithelial-to-mesenchymal transition. PLoS Pathog. 2010;6: e1001170. doi:10.1371/journal.ppat.1001170

22. Teo WH, Chen H-P, Huang JC, Chan Y-J. Human cytomegalovirus infection enhances cell proliferation, migration and upregulation of EMT markers in colorectal cancer-derived stem cell-like cells. Int J Oncol. 2017;51: 1415–1426. doi:10.3892/ijo.2017.4135

23. van Roy F, Berx G. The cell-cell adhesion molecule E-cadherin. Cell Mol Life Sci. 2008;65: 3756–3788. doi:10.1007/s00018-008-8281-1

24. Gumbiner B, Stevenson B, Grimaldi A. The role of the cell adhesion molecule uvomorulin in the formation and maintenance of the epithelial junctional complex. J Cell Biol. 1988;107: 1575–1587. doi:10.1083/jcb.107.4.1575

25. Lewis JE, Wahl JK, Sass KM, Jensen PJ, Johnson KR, Wheelock MJ. Cross-talk between adherens junctions and desmosomes depends on plakoglobin. J Cell Biol. 1997;136: 919–934. doi:10.1083/jcb.136.4.919

26. Moreno-Bueno G, Portillo F, Cano A. Transcriptional regulation of cell polarity in EMT and cancer. Oncogene. 2008;27: 6958–6969. doi:10.1038/onc.2008.346

27. Thiery JP. Epithelial–mesenchymal transitions in development and pathologies. Curr Opin Cell Biol. 2003;15: 740–746. doi:10.1016/j.ceb.2003.10.006

28. Pelaseyed T, Bretscher A. Regulation of actin-based apical structures on epithelial cells. J Cell Sci. 2018;131. doi:10.1242/jcs.221853

29. Bystriansky JS, Kaplan JH. Sodium pump localization in epithelia. J Bioenerg Biomembr. 2007;39: 373–378. doi:10.1007/s10863-007-9100-3

30. Moustakas A, Heldin C-H. Signaling networks guiding epithelial–mesenchymal transitions during embryogenesis and cancer progression. Cancer Sci. 2007;98: 1512–1520. doi:10.1111/j.1349-7006.2007.00550.x

31. Tsubakihara Y, Moustakas A. Epithelial-Mesenchymal Transition and Metastasis under the Control of Transforming Growth Factor β. Int J Mol Sci. 2018;19. doi:10.3390/ijms19113672

32. Abe M, Harpel JG, Metz CN, Nunes I, Loskutoff DJ, Rifkin DB. An assay for transforming growth factor-beta using cells transfected with a plasminogen activator inhibitor-1 promoter-luciferase construct. Anal Biochem. 1994;216: 276–284. doi:10.1006/abio.1994.1042

33. Inman GJ, Nicolás FJ, Callahan JF, Harling JD, Gaster LM, Reith AD, et al. SB-431542 is a potent and specific inhibitor of transforming growth factor-beta superfamily type I activin receptor-like kinase (ALK) receptors ALK4, ALK5, and ALK7. Mol Pharmacol. 2002;62: 65–74. doi:10.1124/mol.62.1.65

34. Buckley ST, Medina C, Ehrhardt C. Differential susceptibility to epithelial-mesenchymal transition (EMT) of alveolar, bronchial and intestinal epithelial cells in vitro and the effect of angiotensin II receptor inhibition. Cell Tissue Res. 2010;342: 39–51. doi:10.1007/s00441-010-1029-x

35. Moser LA, Schultz-Cherry S. Suppression of astrovirus replication by an ERK1/2 inhibitor. J Virol. 2008;82: 7475–7482. doi:10.1128/JVI.02193-07

36. Vu D-L, Bosch A, Pintó RM, Guix S. Epidemiology of Classic and Novel Human Astrovirus: Gastroenteritis and Beyond. Viruses. 2017;9. doi:10.3390/v9020033

37. Finkbeiner SR, Li Y, Ruone S, Conrardy C, Gregoricus N, Toney D, et al. Identification of a novel astrovirus (astrovirus VA1) associated with an outbreak of acute gastroenteritis. J Virol. 2009;83: 10836–10839. doi:10.1128/JVI.00998-09

38. Finkbeiner SR, Holtz LR, Jiang Y, Rajendran P, Franz CJ, Zhao G, et al. Human stool contains a previously unrecognized diversity of novel astroviruses. Virol J. 2009;6: 161. doi:10.1186/1743-422X-6-161

39. Finkbeiner SR, Kirkwood CD, Wang D. Complete genome sequence of a highly divergent astrovirus isolated from a child with acute diarrhea. Virol J. 2008;5: 117. doi:10.1186/1743-422X-5-117

40. Holtz LR, Bauer IK, Rajendran P, Kang G, Wang D. Astrovirus MLB1 is not associated with diarrhea in a cohort of Indian children. PloS One. 2011;6: e28647. doi:10.1371/journal.pone.0028647

41. Meyer CT, Bauer IK, Antonio M, Adeyemi M, Saha D, Oundo JO, et al. Prevalence of classic, MLB-clade and VA-clade Astroviruses in Kenya and The Gambia. Virol J. 2015;12: 78. doi:10.1186/s12985-015-0299-z

42. Vu D-L, Cordey S, Brito F, Kaiser L. Novel human astroviruses: Novel human diseases? J Clin Virol. 2016;82: 56–63. doi:10.1016/j.jcv.2016.07.004

43. Janowski AB, Bauer IK, Holtz LR, Wang D. Propagation of Astrovirus VA1, a Neurotropic Human Astrovirus, in Cell Culture. J Virol. 2017;91. doi:10.1128/JVI.00740-17

44. Hargest V, Davis AE, Tan S, Cortez V, Schultz-Cherry S. Human Astroviruses: A Tale of Two Strains. Viruses. 2021;13. doi:10.3390/v13030376

45. Dermody TS. Orthoreoviruses. 6th ed. Fields Virology. 6th ed. Lippincott Williams and Wilkins; 2013. pp. 1304–1346.

46. McCartney-Francis NL, Frazier-Jessen M, Wahl SM. TGF-β: A Balancing Act. Int Rev Immunol. 1998;16: 553–580. doi:10.3109/08830189809043009

47. Vachon PH, Beaulieu J-F. Transient mosaic patterns of morphological and functional differentiation in the Caco-2 cell line. Gastroenterology. 1992;103: 414–423. doi:10.1016/0016-5085(92)90829-N

48. Guix S, Caballero S, Bosch A, Pintó RM. Human astrovirus C-terminal nsP1a protein is involved in RNA replication. Virology. 2005;333: 124–131. doi:10.1016/j.virol.2004.12.023

49. Guix S, Caballero S, Fuentes C, Bosch A, Pintó RM. Genetic analysis of the hypervariable region of the human astrovirus nsP1a coding region: design of a new RFLP typing method. J Med Virol. 2008;80: 306–315. doi:10.1002/jmv.21058

50. Zha Y, Yao Q, Liu J-S, Wang Y-Y, Sun W-M. Hepatitis B virus X protein promotes epithelial-mesenchymal transition and metastasis in hepatocellular carcinoma cell line HCCLM3 by targeting HMGA2. Oncol Lett. 2018;16: 5709–5714. doi:10.3892/ol.2018.9359

51. Jin Y, Wu D, Yang W, Weng M, Li Y, Wang X, et al. Hepatitis B virus x protein induces epithelial-mesenchymal transition of hepatocellular carcinoma cells by regulating long non-coding RNA. Virol J. 2017;14: 238. doi:10.1186/s12985-017-0903-5

559 52. Li M, Hu L, Zhu F, Zhou Z, Tian J, Ai J. Hepatitis B virus X protein promotes renal epithelial-
560 mesenchymal transition in human renal proximal tubule epithelial cells through the activation of NF-
561 κB. Int J Mol Med. 2016;38: 513–520. doi:10.3892/ijmm.2016.2637

562 53. Hu B, Xie S, Hu Y, Chen W, Chen X, Zheng Y, et al. Hepatitis C virus NS4B protein induces
563 epithelial-mesenchymal transition by upregulation of Snail. Virol J. 2017;14: 83.
564 doi:10.1186/s12985-017-0737-1

565 54. Tiwari I, Yoon M-H, Park B-J, Jang KL. Hepatitis C virus core protein induces epithelial-
566 mesenchymal transition in human hepatocytes by upregulating E12/E47 levels. Cancer Lett.
567 2015;362: 131–138. doi:10.1016/j.canlet.2015.03.032

568 55. Zhou J-J, Meng Z, He X-Y, Cheng D, Ye H-L, Deng X-G, et al. Hepatitis C virus core protein
569 increases Snail expression and induces epithelial-mesenchymal transition through the signal
570 transducer and activator of transcription 3 pathway in hepatoma cells. Hepatol Res Off J Jpn Soc
571 Hepatol. 2017;47: 574–583. doi:10.1111/hepr.12771

572 56. Liu D, Wu J, Liu M, Yin H, He J, Zhang B. Downregulation of miRNA-30c and miR-203a is
573 associated with hepatitis C virus core protein-induced epithelial-mesenchymal transition in normal
574 hepatocytes and hepatocellular carcinoma cells. Biochem Biophys Res Commun. 2015;464: 1215–
575 1221. doi:10.1016/j.bbrc.2015.07.107

576 57. Ranieri D, Belleudi F, Magenta A, Torrisi MR. HPV16 E5 expression induces switching from
577 FGFR2b to FGFR2c and epithelial-mesenchymal transition. Int J Cancer. 2015;137: 61–72.
578 doi:10.1002/ijc.29373

579 58. Zhang W, Wu X, Hu L, Ma Y, Xiu Z, Huang B, et al. Overexpression of Human Papillomavirus Type
580 16 Oncoproteins Enhances Epithelial-Mesenchymal Transition via STAT3 Signaling Pathway in
581 Non-Small Cell Lung Cancer Cells. Oncol Res. 2017;25: 843–852.
582 doi:10.3727/096504016X14813880882288

583 59. Jung Y-S, Kato I, Kim H-RC. A novel function of HPV16-E6/E7 in epithelial-mesenchymal transition.
584 Biochem Biophys Res Commun. 2013;435: 339–344. doi:10.1016/j.bbrc.2013.04.060

585 60. Gaur N, Gandhi J, Robertson ES, Verma SC, Kaul R. Epstein-Barr virus latent antigens EBNA3C
586 and EBNA1 modulate epithelial to mesenchymal transition of cancer cells associated with tumor
587 metastasis. Tumour Biol J Int Soc Oncodevelopmental Biol Med. 2015;36: 3051–3060.
588 doi:10.1007/s13277-014-2941-6

589 61. Morris MA, Laverick L, Wei W, Davis AM, O'Neill S, Wood L, et al. The EBV-Encoded Oncoprotein,
590 LMP1, Induces an Epithelial-to-Mesenchymal Transition (EMT) via Its CTAR1 Domain through
591 Integrin-Mediated ERK-MAPK Signalling. Cancers. 2018;10. doi:10.3390/cancers10050130

592 62. Kim S-M, Oh SW, Park SH, Hur DY, Hong S-W, Han SY. Epstein-Barr virus-encoded latent
593 membrane protein 1 induces epithelial to mesenchymal transition by inducing V-set Ig domain
594 containing 4 (VSIG4) expression via NF-kB in renal tubular epithelial HK-2 cells. Biochem Biophys
595 Res Commun. 2017;492: 316–322. doi:10.1016/j.bbrc.2017.08.116

596 63. Wasil LR, Shair KHY. Epstein-Barr virus LMP1 induces focal adhesions and epithelial cell migration
597 through effects on integrin-α5 and N-cadherin. Oncogenesis. 2015;4: e171.
598 doi:10.1038/oncsis.2015.31

599 64. Chen X, Bode AM, Dong Z, Cao Y. The epithelial-mesenchymal transition (EMT) is regulated by
600 oncoviruses in cancer. FASEB J Off Publ Fed Am Soc Exp Biol. 2016;30: 3001–3010.
601 doi:10.1096/fj.201600388R

65. Marvin S, Meliopoulos V, Schultz-Cherry S. Human Astrovirus Propagation, Purification and Quantification. BIO-Protoc. 2014;4. doi:10.21769/BioProtoc.1078

66. Hargest V, Sharp B, Livingston B, Cortez V, Schultz-Cherry S. Astrovirus Replication Is Inhibited by Nitazoxanide In Vitro and In Vivo. Pfeiffer JK, editor. J Virol. 2020;94: e01706-19. doi:10.1128/JVI.01706-19

67. Subramanian A, Tamayo P, Mootha VK, Mukherjee S, Ebert BL, Gillette MA, et al. Gene set enrichment analysis: A knowledge-based approach for interpreting genome-wide expression profiles. Proc Natl Acad Sci. 2005;102: 15545–15550. doi:10.1073/pnas.0506580102

Figures

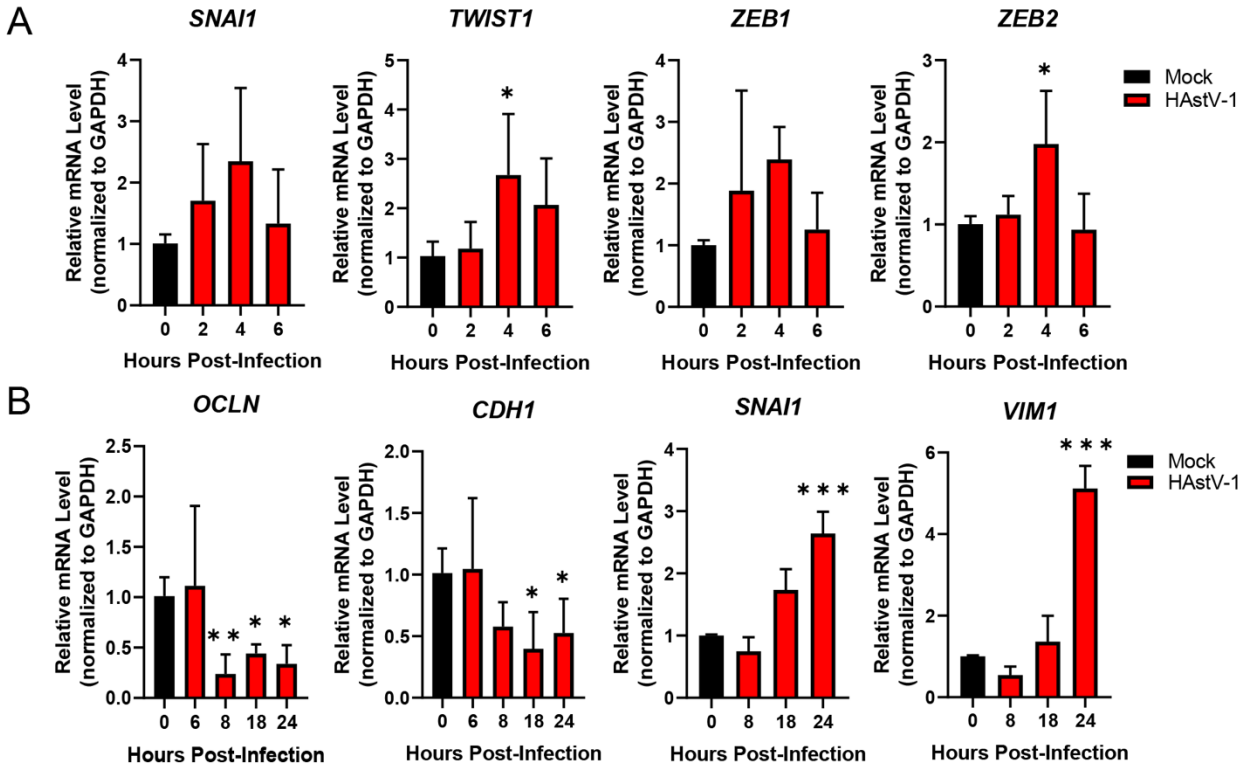

Fig. 1. HAstV-1 infection leads to a decrease in epithelial markers while increasing mesenchymal markers. (A) Early in infection EMT transcription factors (*SNAI1*, *TWIST1*, *ZEB1* and *ZEB2*) are upregulated causing epithelial genes (*OCLN* and *CDH1*) to be down regulated and mesenchymal genes (*SNAI1* and *VIM*) to be upregulated during the course of HAstV-1 infection. Error bars indicate standard deviations from two independent experiments performed in triplicate, and asterisks show statistical significance as measured by Two-way ANOVA followed by Tukey's multiple comparisons test as follows: *, P < 0.05; **, P < 0.01; ***, P < 0.001.

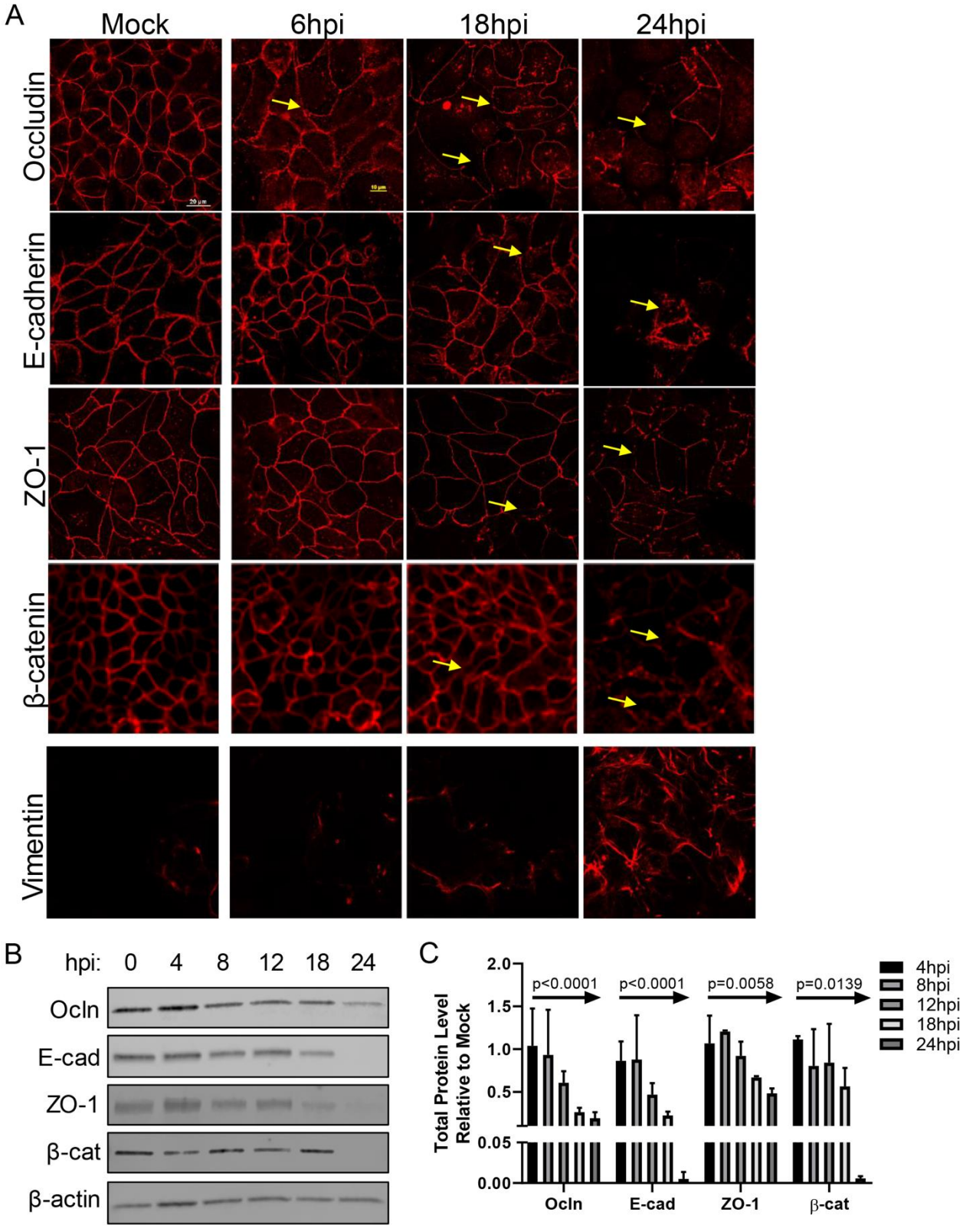

Fig. 2. HAstV-1 infection leads to a time-dependent decrease in junctional protein levels. (A) Caco-2 monolayers on grown coverslips, infected with HAstV-1 (MOI

of 10) or mock infected. Cells were fixed at 6, 18, and 24 hpi in 4% paraformaldehyde and then stained for the indicated junctional proteins. Arrows indicate areas of junctional disruption. Images are representative of at least three independent experiments. (B) Expression of epithelial markers, occludin (Ocln), E-cadherin (E-cad), ZO-1, and β-catenin (β-cat), were quantified by immunoblot of HAstV-1 or mock infected Caco-2 cell lysates. (C) Bands were then quantified by densitometry and normalized to β-actin then compared to mock-infection. Error bars indicate standard deviations three independent experiments performed in duplicate, p-value as measured by Ordinary One-way ANOVA followed by a test for trend is indicated for each protein.

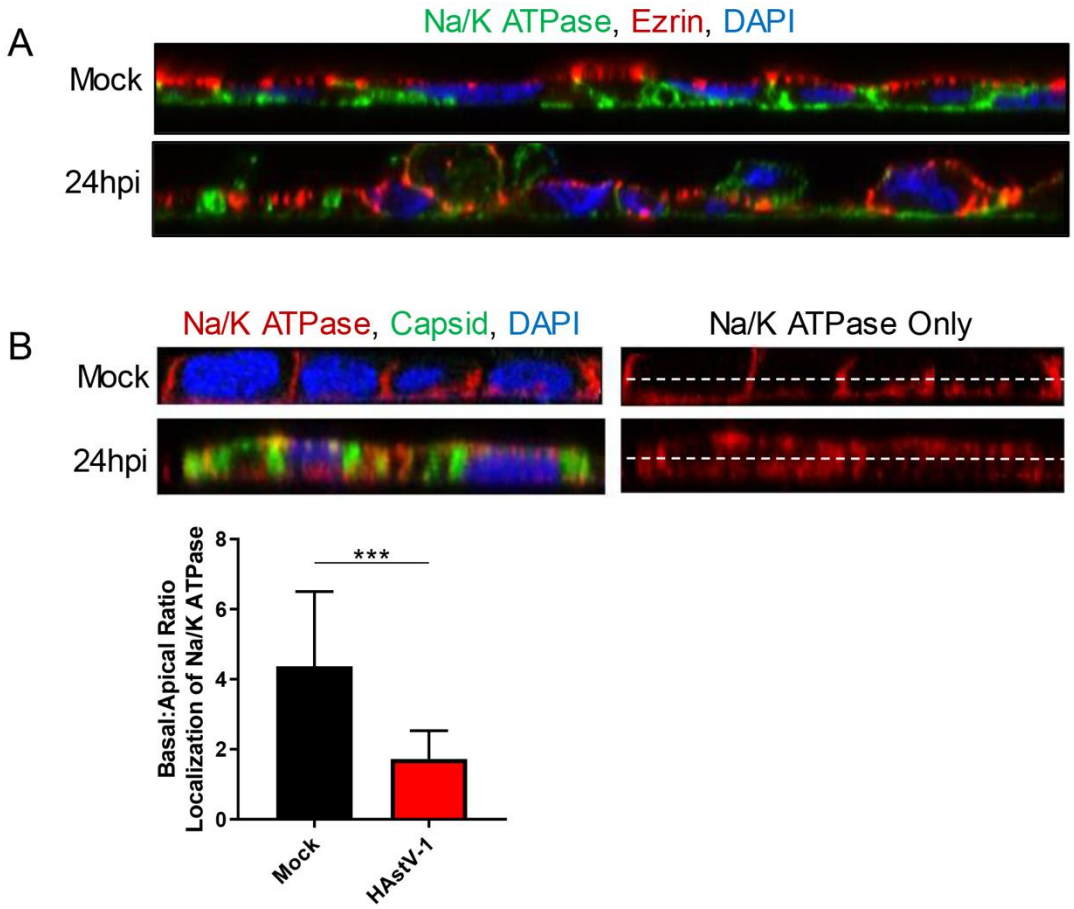

Fig. 3. HAstV-1 infection leads to a disruption of cellular polarity. (A) Caco-2 infected with HAstV-1 or mock infected (as indicated). Cells were fixed at 24 hpi in 100% ice-cold methanol and then stained for ezrin (red), sodium-potassium ATPase (green), and DAPI (blue). Images are representative of at least three independent experiments. (B) Basal or apical localization of sodium-potassium ATPase was determined by measuring intensity above and below cell midline of HAstV- or mock-infected cells using ImageJ. Error bars indicate standard deviations of three independent experiments performed in triplicate, and asterisks show statistical significance as measured by the two-tailed Student *t* test as follows: *, $P < 0.05$; **, $P < 0.01$; ***, $P < 0.001$.

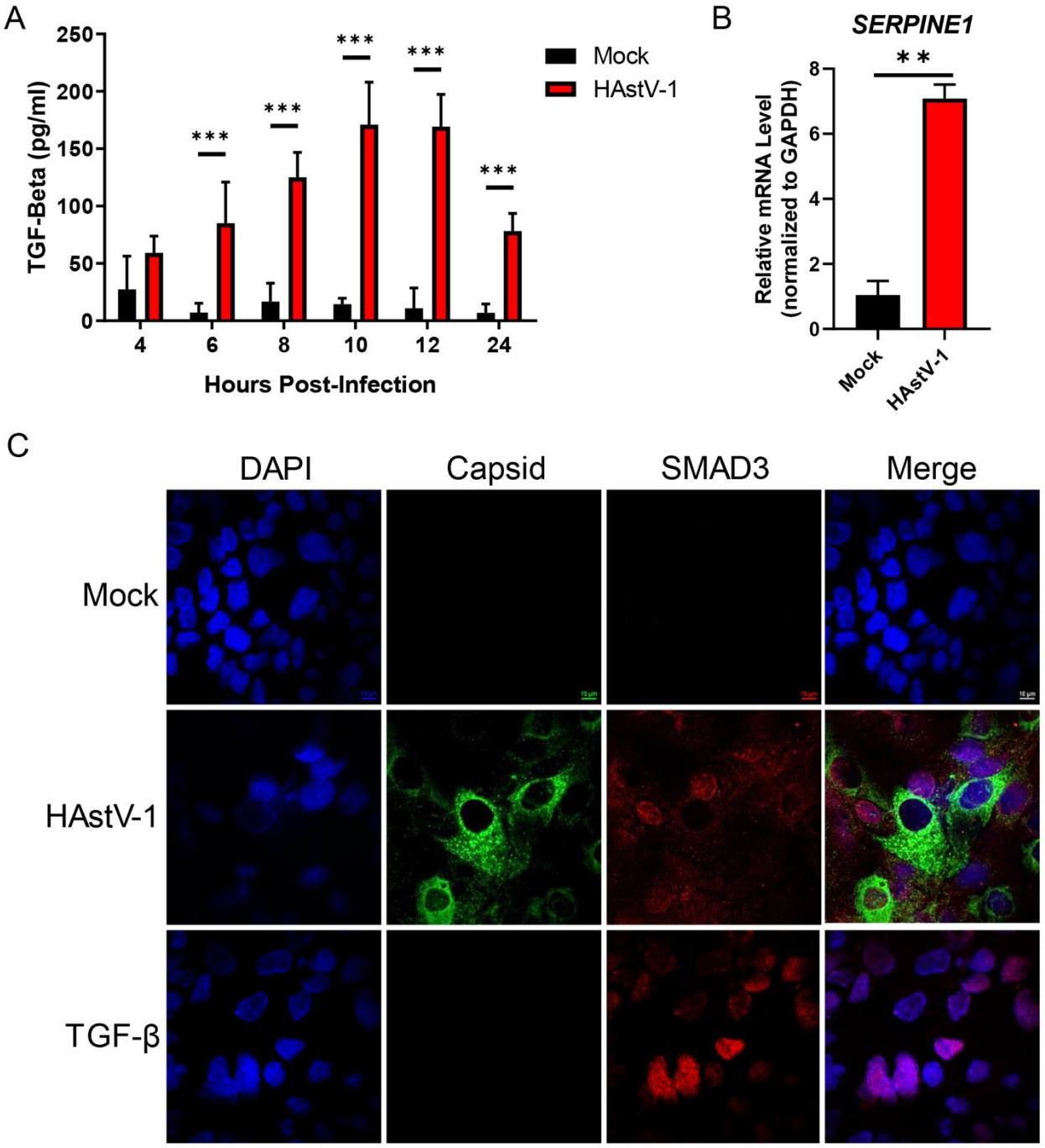

Fig. 4. TGF-β activity increases during the course of HAstV-1 infection. (A) Supernatants were collected from Caco-2 infected with HAstV-1 or mock infected

from 4 to 24 hpi. Supernatants were then assayed for active TGF-β using the PAI assay as described previously [32]. Error bars indicate standard deviations from two independent experiments performed in duplicate, and asterisks show statistical significance as measured by two-way ANOVA followed by Sidak's multiple comparisons test as follows: *, P < 0.05; **, P < 0.01; ***, P < 0.001. (B) *SERPINE1*, which is specifically activated by TGF-β, mRNA levels were measured in mock infected or HAstV-1 infected Caco-2 cells at 24 hpi. Error bars indicate standard deviations from two independent experiments performed in duplicate, and asterisks show statistical significance as measured by the two-tailed Student *t* test as follows: *, P < 0.05; **, P < 0.01; ***, P < 0.001. (C) Caco-2 cells mock infected, HAstV-1 infected, or treated with 20ng/ml of TGF-β stained for SMAD3 (red), astrovirus capsid protein (green) and DAPI (blue). Images are representative of two independent experiments.

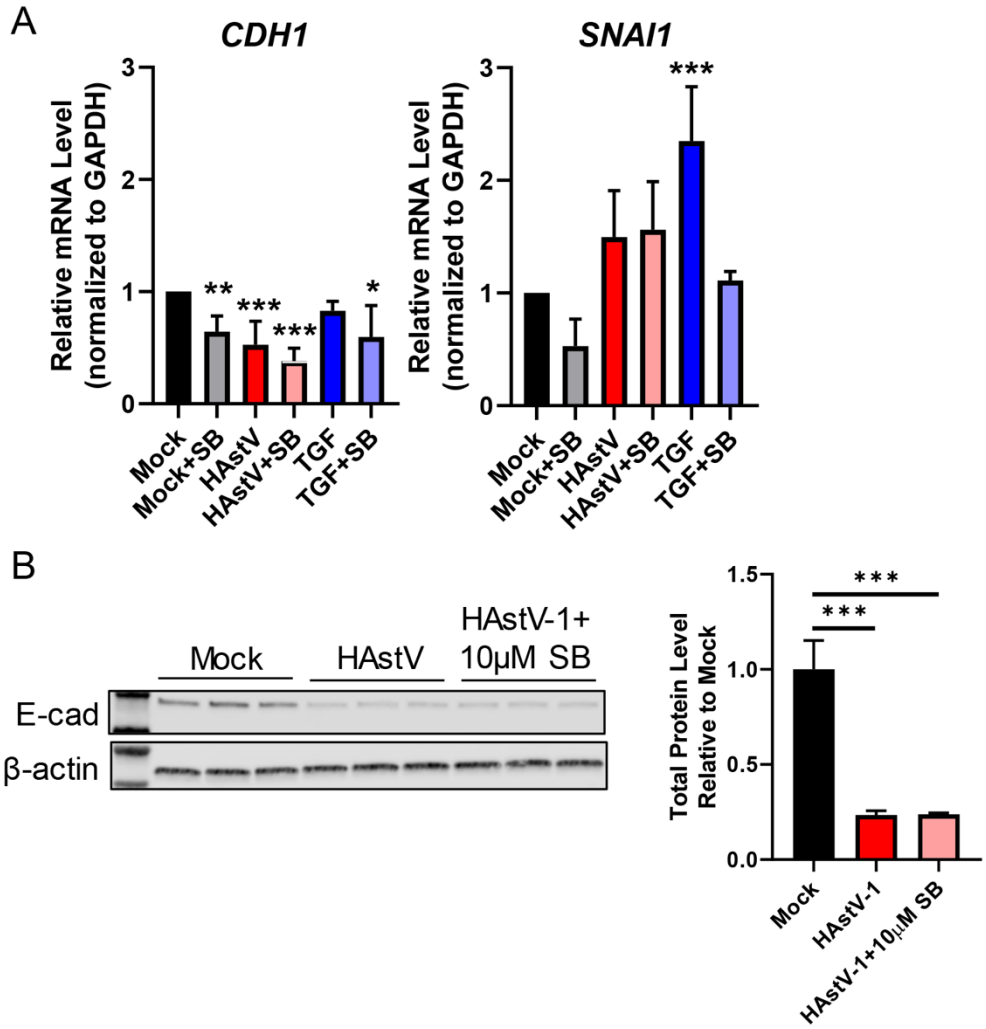

Fig. 5. Inhibition of TGF-β signaling with SB431542 does not inhibit HAstV-1 induced EMT. (A) RNA extracted at 24 hpi from Caco-2 cells infected with HAstV-1, TGF-β treated, or mock infected with or without 10μM SB431542 shows

SB431542 does not rescue *CDH1* or *SNAI1* regulation in HAstV-induced EMT. (B) Expression of epithelial marker, E-cadherin, was quantified by immunoblot of HAstV-1 or mock infected Caco-2 cell lysates with or without 10μM SB431542. Bands were then quantified by densitometry and normalized to β-actin then compared to mock-infection. All error bars indicate standard deviations of two independent experiments performed in triplicate, and asterisks show statistical significance as measured by ordinary one-way ANOVA followed by Dunnett's multiple comparisons test as follows: *, $P < 0.05$; **, $P < 0.01$; ***, $P < 0.001$.

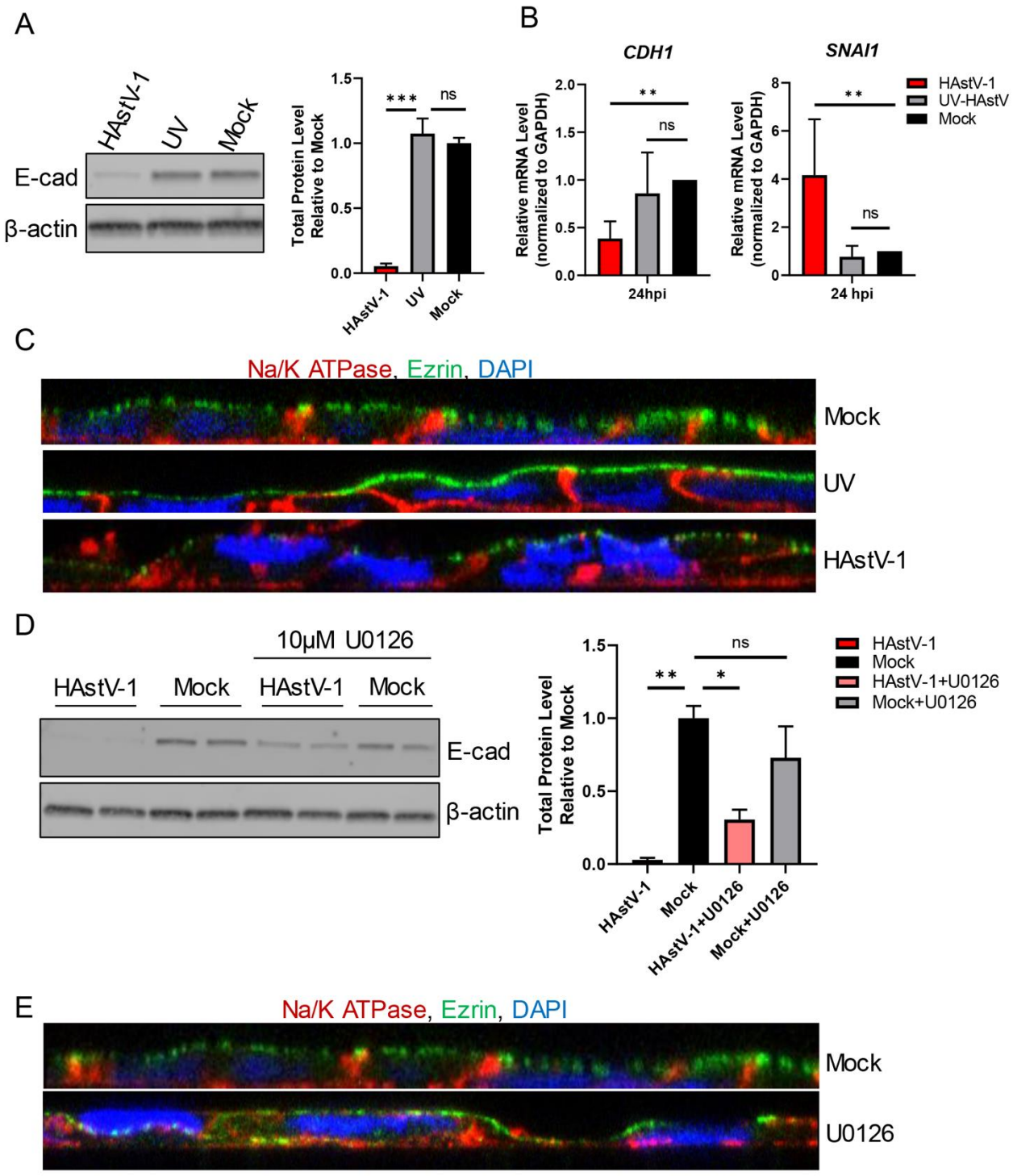

Fig. 6. Replication is required for HAstV-1 induced EMT. (A) Expression of E-cadherin was quantified by immunoblot of HAstV-1, UV-inactivated HAstV-1, or mock infected Caco-2 cell lysates. Bands were then quantified by densitometry and normalized to β-actin then compared to mock-infection. (B) RNA extracted at 24 hpi from Caco-2 cells infected with HAstV-1, UV-inactivated HAstV-1, or mock infected show UV-inactivated virus does not modulate *CDH1* or *SNAI1* regulation as active HAstV-1 does. (C) Na/K ATPase (red) and ezrin (green) localization in Caco-2 cells inoculated with UV-inactivated HAstV-1 shows no difference to mock infected cells. (D) Expression of E-cadherin was quantified by immunoblot of HAstV-1, HAstV-1 + 10μM U0126, or mock infected Caco-2 cell lysates. Bands were then quantified by densitometry and normalized to β-actin then compared to mock-infection. (E) Na/K ATPase (red) and ezrin (green) localization in Caco-2 cells infected with HAstV-1 in the presence of 10μM U0126 and mock infected cells. All error bars indicate standard deviations of three independent experiments performed in triplicate, and asterisks show statistical significance as measured by ordinary one-way ANOVA followed by Dunnett's multiple comparisons test as follows: *, $P < 0.05$; **, $P < 0.01$; ***, $P < 0.001$.

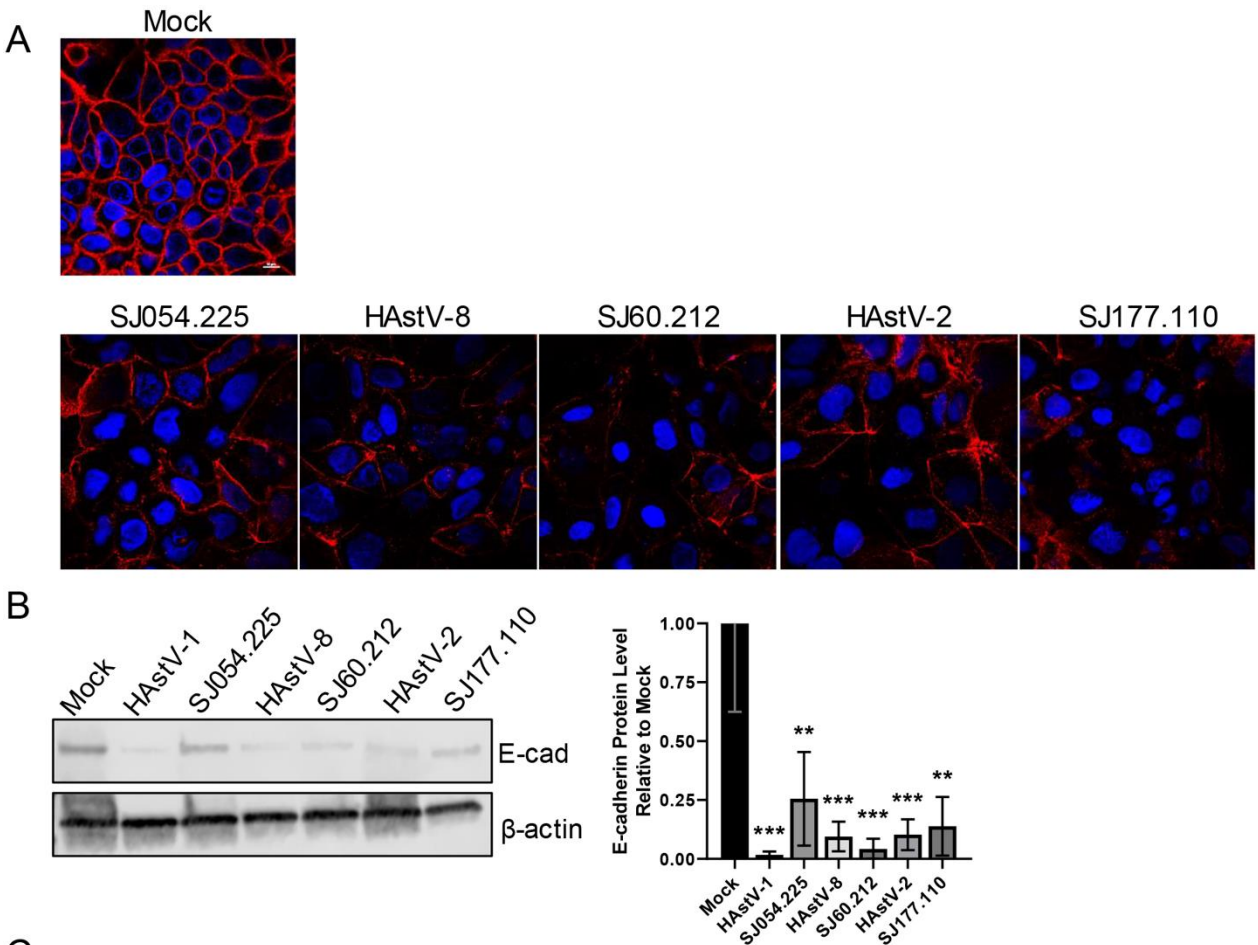

720
721
722
723

724 **Fig. 7. Multiple HAstV serotypes and clinical isolates induce EMT.** (A) Caco-2
725 monolayers on grown coverslips, infected with HAstV-1 (lab-adapted), SJ054.225
726 (HAstV-1 isolate), HAstV-8 (lab-adapted), SJ60.212 (HAstV-8 isolate), HAstV-2
727 (lab-adapted), SJ177.110 (HAstV-2 isolate) or mock infected. Cells were fixed at
728 24hpi and stained for E-cadherin (red) and DAPI (blue). (B) Expression of E-
729 cadherin was quantified by immunoblot of HAstV-1 (lab adapted), SJ054.225
730 (HAstV-1 isolate), HAstV-8 (lab adapted), SJ60.212 (HAstV-8 isolate), HAstV-2
731 (lab adapted), SJ177.110 (HAstV-2 isolate) infected (MOI of 10) or mock infected
732 Caco-2 cell lysates. Bands were then quantified by densitometry and normalized
733 to β-actin then compared to mock-infection. Error bars indicate standard
734 deviations of two independent experiments performed in triplicate, and asterisks
735 show statistical significance as measured by ordinary one-way ANOVA followed
736 by Dunnett's multiple comparisons test as follows: *, $P < 0.05$; **, $P < 0.01$; ***, P
737 < 0.001. (C) Na/K ATPase (red) and ezrin (green) localization in Caco-2 cells
738 infected with lab adapted and clinical isolate HAstVs is disrupted compared to
739 mock infected cells. All images are representative of two independent
740 experiments.
741

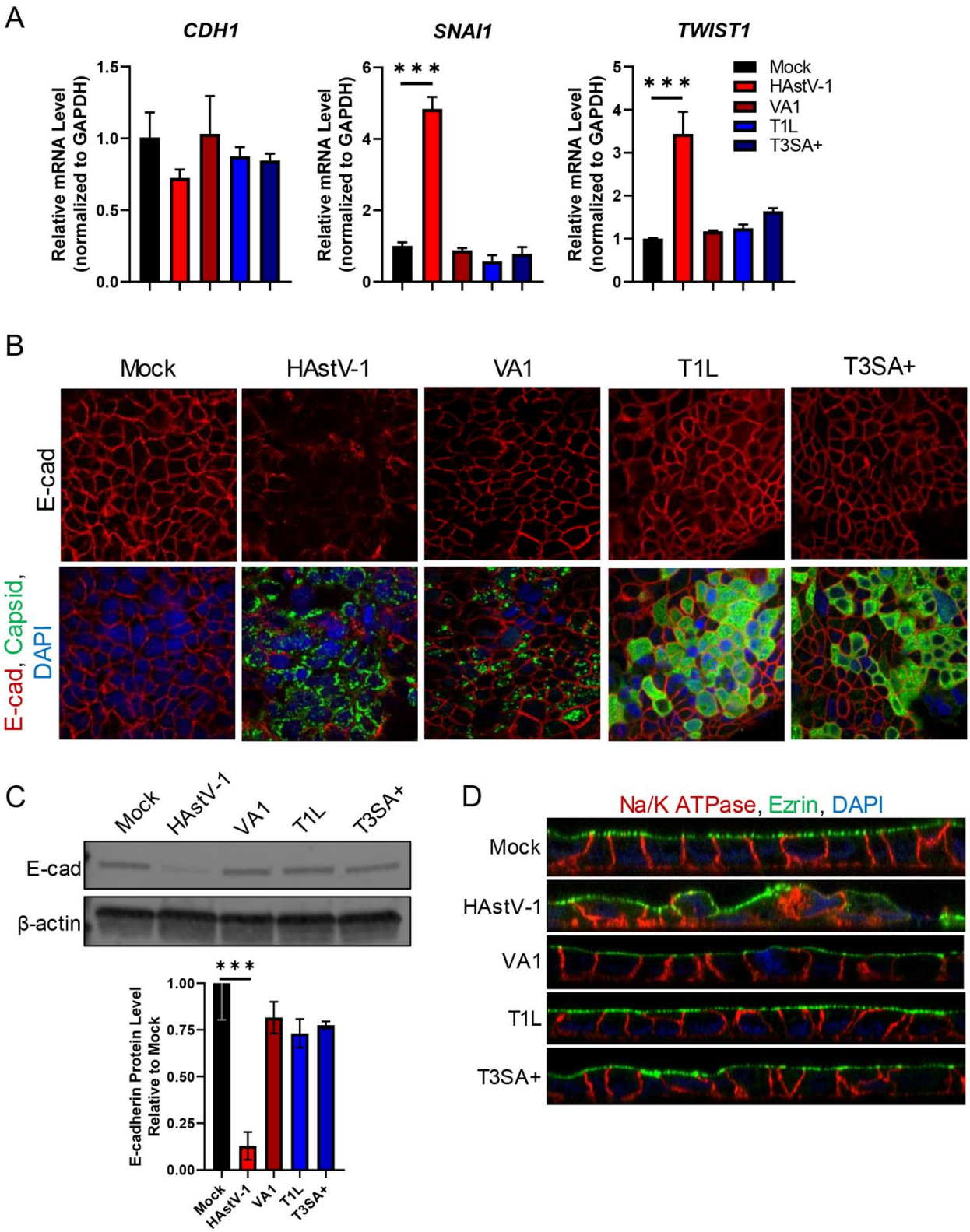

Fig. 8. Other enteric viruses do not induce EMT in Caco-2 cells. (A) Caco-2 monolayers grown on permeable supports were infected with HAstV-1, HAstV-VA1, T1L, T3SA+ (MOI of 10) or mock-infected and TER (transepithelial electrical resistance) was measured from 0-24 hpi. (B) RNA extracted at 24 hpi from Caco-2 cells infected with HAstV-1, HAstV-VA1, T1L, T3SA+, or mock infected, show only HAstV-1 modulate *CDH1*, *SNAI1*, and *TWIST1*. (C) Infected cells were fixed at 24hpi and stained for E-cadherin (red), viral capsid (green), and DAPI (blue). (D) Expression of E-cadherin was quantified by immunoblot of HAstV-1, HAstV-VA1, T1L, T3SA+ infected (MOI of 10) or mock infected Caco-2 cell lysates. Bands were then quantified by densitometry and normalized to β-actin then compared to mock-infection. (E) Na/K ATPase (red) and ezrin (green) localization is disrupted in cells infected with HAstV-1 compared to HAstV-VA1, T1L, T3SA+, and mock infected cells. All error bars indicate standard deviations of two independent experiments performed in triplicate, and asterisks show statistical significance as measured by ordinary one-way ANOVA followed by Dunnett's multiple comparisons test as follows: *, P < 0.05; **, P < 0.01; ***, P < 0.001. All images are representative of two independent experiments.

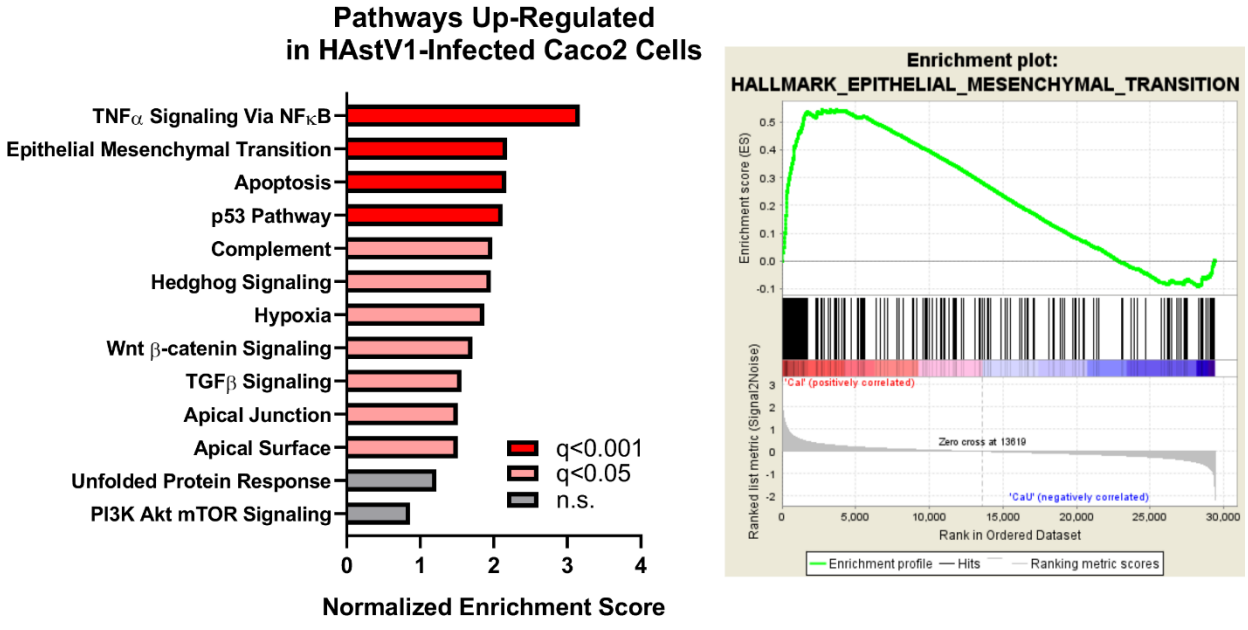

Fig. S1. EMT pathway is upregulated in HAstV-infected Caco-2 cells. Gene set enrichment analysis was performed on HAstV-infected (MOI of 10) and uninfected Caco-2 intestinal epithelial cells. Shown are top upregulated hallmark pathways' normalized enrichment scores with false discovery rate estimated by Benjamin-Hochberg method cut-offs of q<0.001 (red), q<0.05 (blue), and q>0.05 or non-significant (gray).

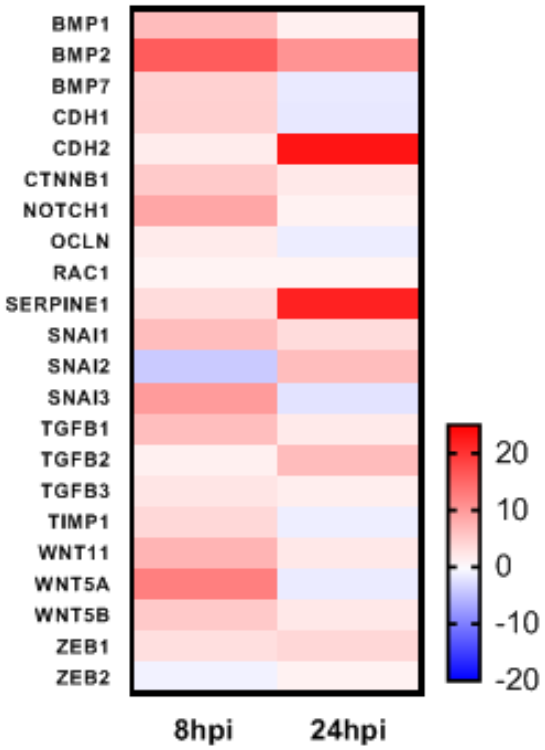

Fig. S2. EMT-associated genes modulated by HAstV infection. Heatmap showing fold regulation of EMT associated genes from Qiagen's RT2 Profiler PCR Array Human Epithelial to Mesenchymal Transition (EMT). RNA samples were collected from HAstV-infected or mock-infected cells at 8 and 24 hpi. Gene expression values are colored corresponding to the up (red) or downregulation (blue) relative to mock-infected cells.

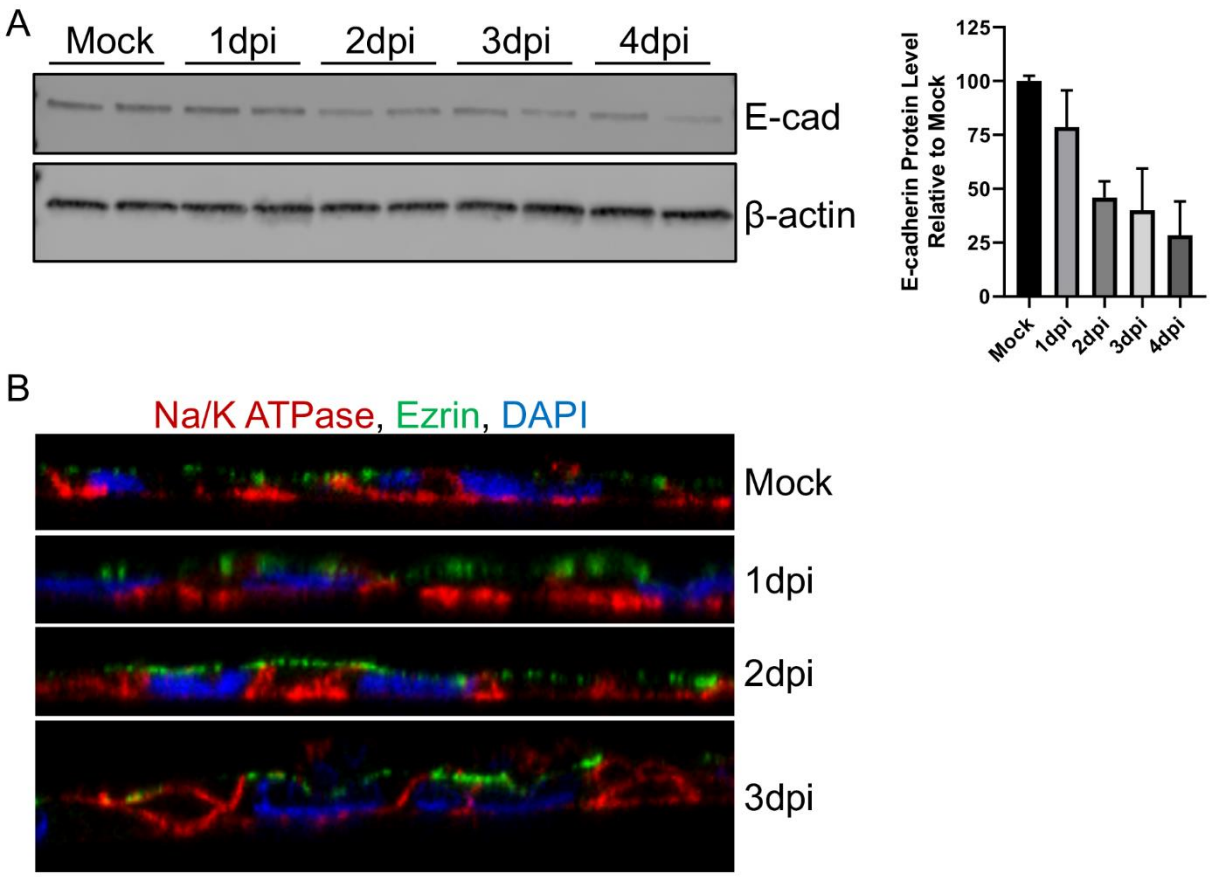

Fig. S3. TGF-β induced EMT in Caco-2 cells. (A) Western blot of E-cadherin at 1, 2, 3, and 4 days post inoculation with 20 ng/ml active TGF-β compared to mock. Bands were quantified by densitometry and normalized to β-actin then compared to mock-infection. (B) Caco-2 inoculated with 20ng/ml active TGF-β or mock treated (as indicated). Cells were fixed at 1, 2, or 3 days post-inoculation in 100% ice-cold methanol and then stained for ezrin (green), Na/K ATPase (red), and DAPI (blue).

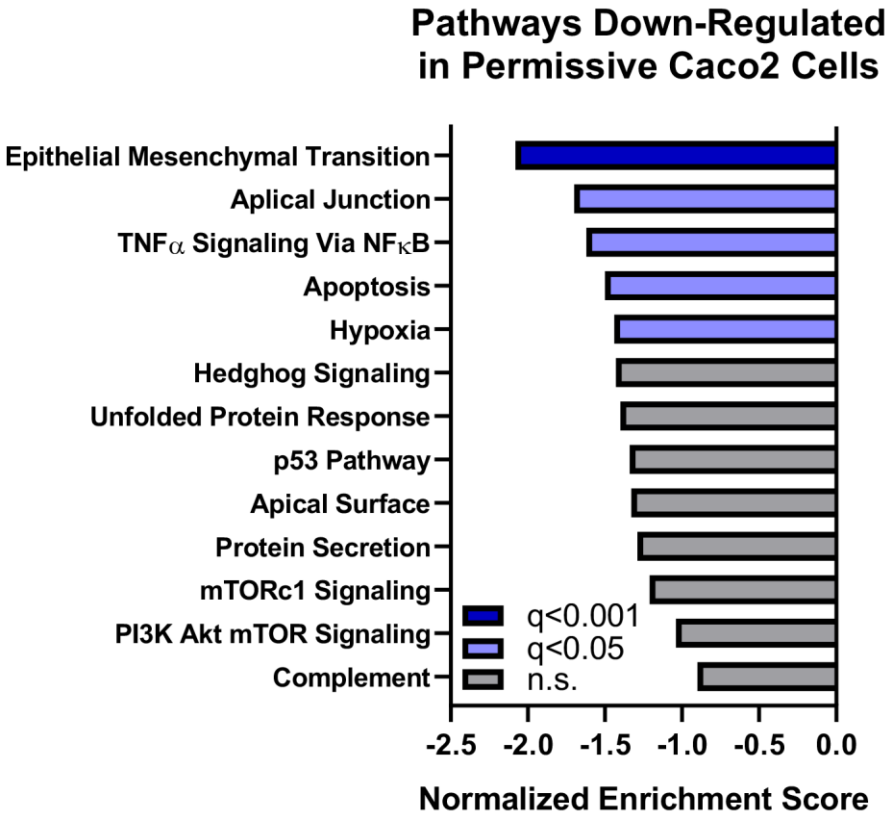

794

795 **Fig. S4. EMT pathway is downregulated in permissive Caco-2 cells at baseline.**
796 Gene set enrichment analysis was performed on differentiated and sub-confluent
797 uninfected Caco-2 intestinal epithelial cells. Shown are top downregulated
798 hallmark pathways' normalized enrichment scores with false discovery rate
799 estimated by Benjamin-Hochberg method cut-offs of q<0.001 (red), q<0.05
800 (blue), and q>0.05 or non-significant (gray).

801

802